A Framework for Performing Multiscale Stochastic Progressive Failure Analysis of Composite Structures

Brett A. Bednarcyk[1] and Steven M. Arnold[2]

[1]Ohio Aerospace Institute, Cleveland, OH 44142

[2]NASA Glenn Research Center, Cleveland, OH 44135

Abstract: A framework is presented that enables coupled multiscale analysis of composite structures. The recently developed, free, Finite Element Analysis – Micromechanics Analysis Code (FEAMAC) software couples the Micromechanics Analysis Code with Generalized Method of Cells (MAC/GMC) with ABAQUS to perform micromechanics based FEA such that the nonlinear composite material response at each integration point is modeled at each increment by MAC/GMC. As a result, the stochastic nature of fiber breakage in composites can be simulated through incorporation of an appropriate damage and failure model that operates within MAC/GMC on the level of the fiber. Results are presented for the progressive failure analysis of a titanium matrix composite tensile specimen that illustrate the power and utility of the framework and address the techniques needed to model the statistical nature of the problem properly. In particular, it is shown that incorporating fiber strength randomness on multiple scales improves the quality of the simulation by enabling failure at locations other than those associated with structural level stress risers.

Keywords: Composites, Constitutive Model, Coupled Analysis, Curtin Model, Damage, Failure, FEAMAC, Fiber Breakage, ImMAC, MAC/GMC, Micromechanics, Plasticity, Probabilistic Design, Titanium Matrix Composites, Viscoplasticity.

1. Introduction

The Integrated Multiscale Micromechanics Analysis Code (ImMAC) Software Suite consists of three components for the design and analysis of composite structures (see Fig. 1): 1) the Micromechanics Analysis Code with Generalized Method of Cells (MAC/GMC) performs rapid, stand alone analysis of composite materials and laminates based on non-FEA micromechanics methods; 2) Finite Element Analysis – Micromechanics Analysis Code (FEAMAC) couples the efficient micromechanics capabilities of MAC/GMC with the ABAQUS finite element code for multiscale analysis of composite structures; and 3) HyperMAC couples the MAC/GMC micromechanics capabilities with the HyperSizer stiffened structural optimization software

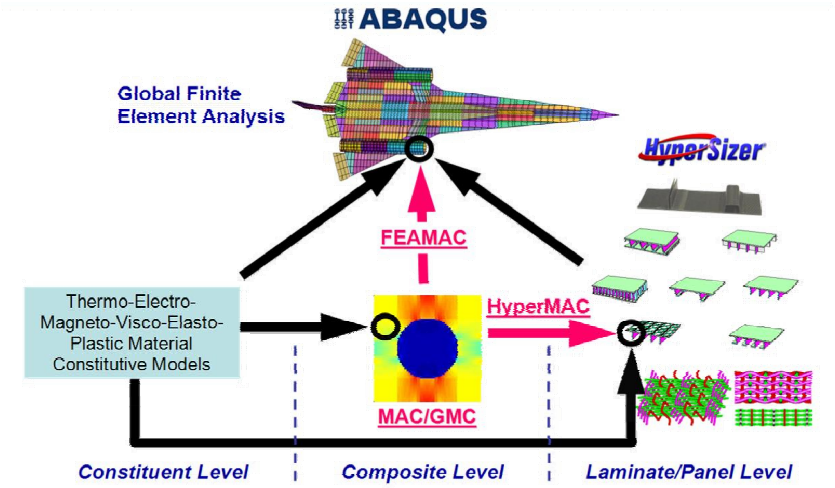

Figure 1. Overview of the NASA GRC/OAI ImMAC Software Suite.

(Collier Research Corp., 2005). This paper focuses on the FEAMAC software, in which the generalized method of cells (GMC) micromechanics approach is used to model the local composite material behavior at the integration points within each finite element comprising a composite structure via the ABAQUS user-definable subroutines. GMC localizes to the level of the fiber and matrix constituent materials, and thus enables the use of arbitrary nonlinear constitutive, damage, and life models (many of which are provided by MAC/GMC) for each monolithic constituent phase throughout the composite structure. This circumvents the need for the development and characterization of effective anisotropic constitutive models for the composite materials within the structure, which can be a difficult task in the presence of material nonlinearity. Further, GMC provides access to the constituent level stresses and strains throughout the structure, enabling the use of fiber and matrix scale failure and damage evolution criteria. The well-documented computational efficiency of the GMC micromechanics approach (as compared to the finite element micromechanics approach, for example) (Wilt, 1995; Pindera and Bednarcyk, 1999) is an important asset that permits the tractability of coupled structural FEA-micromechanics problems.

This investigation is intended to highlight the critical ingredients required to account properly for the stochastic nature of fiber failure within the context of a multiscale analysis. The results are purposely qualitative in nature, as opposed to representing a rigorous comparison of the method's predictions with experimental results. Such studies are planned as future work. Herein a simple nonlinear composite structure is considered, namely, a titanium matrix composite tensile test specimen. Through FEAMAC's multiscale approach, an accurate fiber strength distribution can be represented and assigned to the ABAQUS model geometry. It is shown that the effects of fiber strength variability should be included not only at the micro scale, but also at the structural scale. This enables realistic simulation of the stochastic structural failure phenomenon, wherein failure does not necessarily initiate at the highest structural level stress concentration.

2. Description of the Modeling Framework

The four levels of scale encompassed by the ImMAC software suite are depicted in Fig. 1. The ABAQUS finite element software operates on the highest structural scale, providing the global solution to the problem. Through the FEAMAC software (described in more detail below), composite materials at the integration points within each element can be represented via the MAC/GMC software. Within MAC/GMC, the behavior of each phase (i.e., the fiber and the matrix materials) can be modeled using advanced nonlinear constitutive, damage, and failure models. This multiscale framework provides a consistent and tractable platform for performing high-fidelity simulations that rely on physics-based methods on all applicable scales. Also shown in Fig. 1 is the HyperMAC software, which couples MAC/GMC to the HyperSizer commercial stiffened structural sizing software. Note that HyperSizer does not explicitly link with ABAQUS at this time, although it does link with other commercial FEA software.

2.1 FEAMAC

The new FEAMAC implementation, which couples the composite material model provided by MAC/GMC with ABAQUS structural models, is shown schematically in Fig. 2. The software relies on four basic ABAQUS user defined subroutines. For the mechanical analysis, the `UMAT` subroutine is called for a given integration point (at a given increment and iteration) and provides the strains, strain increments, and current values of the state variables to MAC/GMC through a front end subroutine called `FEAMAC`. MAC/GMC then returns to ABAQUS a new stiffness and stress state for the integration point based on the strain increment. For the thermal analysis, the `UEXPAN` subroutine is called, providing the integration point temperature, temperature increment, and current state to MAC/GMC and then obtaining new thermal strains and thermal strain rates.

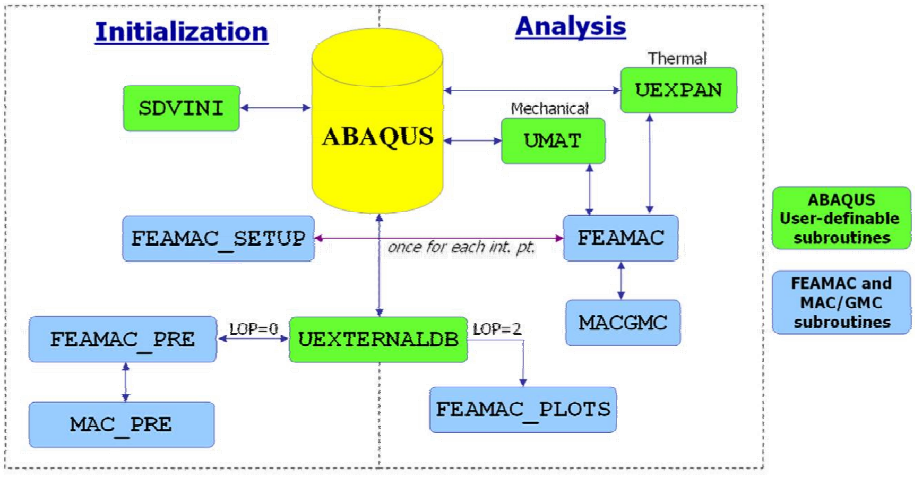

Figure 2. Overview of the FEAMAC software implementation.

The user subroutine `UEXTERNALDB` is used for problem set up tasks and for writing MAC/GMC level output data to files. Finally, the user subroutine `SDVINI` is used for problem initialization tasks. The ABAQUS user defined subroutines shown in Fig. 2 are provided to FEAMAC users as a Fortran source file, while the FEAMAC and MAC/GMC subroutines depicted are provided as a static library that is linked with ABAQUS at run time.

In order to set up an FEAMAC problem, a standard ABAQUS input file is used that includes a user material with a name ending in either "`.mac`" or "`_mac`". These extensions indicate to FEAMAC that the material is a MAC/GMC composite material whose constituent properties and architecture (e.g., fiber volume fraction and fiber arrangement) are defined in a MAC/GMC input file of the same name. The applicable MAC/GMC input file(s) must be located in the same directory as the ABAQUS input file. Materials that are not associated with MAC/GMC are also permitted in FEAMAC problems. The ABAQUS input file will also typically include an orientation definition (as composite materials are usually anisotropic), while the necessary cards usually associated with a user material must be specified as well. Only one additional card, not typically associated with a user material problem must be specified in order to trigger certain initialization tasks: `*INITIAL CONDITIONS, TYPE=SOLUTION, USER`. FEAMAC problem execution is accomplished identically to any problem that utilizes a user material, wherein the Fortran source file containing the appropriate user subroutines is specified. Finally, FEAMAC problem post processing is accomplished identically to any ABAQUS problem, as all typical ABAQUS output, including the `.odb` file, is available. Constituent level field variables are stored internally within the ABAQUS state variable space and are also available for post-processing.

2.2 MAC/GMC

The Micromechanics Analysis Code with Generalized Method of Cells (MAC/GMC) (Bednarcyk and Arnold, 2002) is a micromechanics analysis package, based on the generalized method of cells (GMC) multi-axial micromechanics approach (Paley and Aboudi, 1992), with many features that render it user-friendly and widely-applicable. It can simulate the nonlinear behavior and life of a wide range of composites and laminates, including MMCs, PMCs, CMCs, and smart materials and composites.

The GMC method is not based on the finite element method, but rather relies on a semi-closed form continuum mechanics theory. Through localization and homogenization, it provides an effective nonlinear constitutive equation for a composite material based on the behavior and arrangement of the constituent materials of the form,

$$\overline{\boldsymbol{\sigma}} = \mathbf{C}^{*}\left(\overline{\boldsymbol{\varepsilon}} - \overline{\boldsymbol{\varepsilon}}^{I} - \overline{\boldsymbol{\varepsilon}}^{T}\right) \tag{1}$$

where $\mathbf{C}^{*}$ is the composite level effective stiffness matrix, $\overline{\boldsymbol{\sigma}}$ is the composite level stress vector, and $\overline{\boldsymbol{\varepsilon}}$, $\overline{\boldsymbol{\varepsilon}}^{I}$, and $\overline{\boldsymbol{\varepsilon}}^{T}$ are the composite level total, inelastic, and thermal strain vectors, respectively. The composite material is treated as periodic in either two or three directions, and a repeating unit cell (RUC) is identified that represents the composite material microstructure. The RUC is then divided into an arbitrary number of subcells, each of which may be assigned a

distinct material. Because GMC localizes to the level of the individual constituent materials, the local fiber and matrix stress and strain fields are available throughout the composite material. This allows models for nonlinear effects such as inelasticity, damage, and failure to be incorporated on this local scale, which means these local models apply to monolithic rather than composite materials. Obviously, such models that apply to monolithic, and usually isotropic, materials are much simpler to formulate and characterize, and a great number are readily available. Within GMC, damage is manifested through the $\mathbf{C}^*$ and $\bar{\boldsymbol{\varepsilon}}^I$ terms in Eq. (1), as a reduction and increase in magnitude, respectively.

MAC/GMC also includes a laminate analysis module in which each ply is modeled as a nonlinear GMC composite material. The software has been applied extensively in the literature (Aboudi, 2004) and has been shown to be accurate, robust, and efficient. MAC/GMC is available for free to the public from NASA Glenn Research Center (as is FEAMAC), and its capabilities are ever expanding.

2.3 Matrix Material Viscoplasticity: GVIPS Model

In order to simulate the inelastic behavior of the matrix in the metal matrix composite specimen analyzed herein, an inelastic constitutive model was employed. This model then provides the local inelastic strains at a point within each subcell comprising the micromechanics model RUC.

The titanium matrix alloy considered herein (Ti-21S) is simulated using a generalized viscoplasticity with potential structure (GVIPS) model (Arnold et al., 1994). This physics-based, multi-axial, nonisothermal, fully associative, unified, viscoplastic model is based on Gibb's complementary free energy and complementary dissipation potentials, and includes nonlinear kinematic hardening. GVIPS is quite robust and able to simulate accurately the response of the titanium over a full range of arbitrary, time-dependent, local stress states. Although all of these features are not necessarily required for this particular study, the model was used because of its availability in MAC/GMC.

2.4 Stochastic Fiber Breakage: Curtin Model

Curtin's (1991) effective fiber breakage model was employed to account for the stochastic effects of fiber breakage in the composite material. The Curtin model was incorporated within GMC by Bednarcyk and Arnold (2001) and shown to be as effective (but more efficient) than Monte Carlo-like simulations for modeling the longitudinal tensile response of SiC/Ti-21S composites at the material level. Using fiber strength statistics combined with a shear-lag analysis, Curtin (1991) developed an equation describing the stiffness degradation of an effective fiber that represents all fibers in a composite material as the composite is loaded longitudinally. The effective fiber elastic modulus is given by,

$$E_f^* = \frac{1}{2}\left\{1+\exp\left[-\left(\frac{E_f\,\varepsilon_f^{mech}}{\sigma_c}\right)^{m+1}\right]\right\}E_f \tag{2}$$

where E_f is the original fiber modulus, ε_f^{mech} is the fiber longitudinal mechanical strain, m is the

fiber Weibull modulus, and $\sigma_c = \left(2\sigma_0^m \tau L_0 / d\right)^{1/(m+1)}$. The term σ_0 is the characteristic fiber strength, τ is the frictional sliding resistance between the fiber and the matrix, L_0 is the fiber gauge length, and *d* is the fiber diameter. The model predicts complete fiber failure when the stress in the effective fiber reaches a maximum,

$$\sigma_f^{\max} = \frac{1}{2}\sigma_c x^{1/(m+1)}\left[1+\exp(-x)\right] \tag{3}$$

where x is the first positive number that satisfies,

$$1+\left[1-(m+1)x\right]\exp(-x) = 0 \tag{4}$$

Based on the fiber strength histogram parameters, the Curtin model predicts that the effective fiber will first load up elastically and eventually begin to damage, resulting in a loss of stiffness. Complete fiber failure is then signaled by the fiber stress reaching a peak value.

3. Results and Discussion

The focus of the presented results is the stochastic analysis of the fiber breakage dominated progressive failure process in longitudinally-reinforced SiC/Ti metal matrix composite (MMC) structures. In particular, we consider perhaps the simplest (yet extremely important) composite structure: an experimental tensile test specimen. Such test specimens are critical to both materials scientists and structural engineers because they are used to evaluate material quality during development of materials and to characterize material parameters needed for structural analysis. The design of test specimens is also known to be critical so as to ensure a uniform state of stress and strain in the gauge section, as well as consistent failure within the gauge section. In the case of MMCs, obtaining adequate specimen designs has proven more challenging (compared to monolithic metals) because of their anisotropy and the tendency of the fibers to provide a conduit for local information, such as the effects of a stress concentration (Worthem, 1990; Spencer, 1972).

Research on MMC testing at NASA Glenn Research Center in the 1990s arrived at an acceptable specimen design (Bowman, 1999; Lerch, 2005), shown in Fig. 3, which has been adopted in the current analytical study. As shown, the specimen (commonly referred to as a "dogbone specimen") has a reduced gauge section that concentrates the stress and strain in order to induce failure in the gauge section. As shown by Worthem (1990), a common problem with test specimens of this shape is failure at the transition between the reduction and gauge sections (as indicated by the dotted lines in Fig. 3). This is due to a shape-induced local stress concentration occurring at the specimen free edge in this region. By using a very large radius for the reduction, such as 14.5 in., this problem can be minimized and specimen failure consistently achieved within the gauge section as desired. This is illustrated in Fig. 4(a), which shows 6 failed longitudinal SiC/Ti-21S tensile test specimens and Fig. 4(b), which shows a plot of the length of the longer part

of the failed specimens. While there is significant variation of the failure location, all six specimens failed well within the gauge section

To analyze the SiC/Ti tensile specimen shown in Fig. 3, we consider a one eighth symmetry 3D ABAQUS model consisting of 300 C3D8 elements, as shown in Fig. 5. Symmetry was used for convenience and to minimize execution times. Note that a mesh sensitivity study was performed

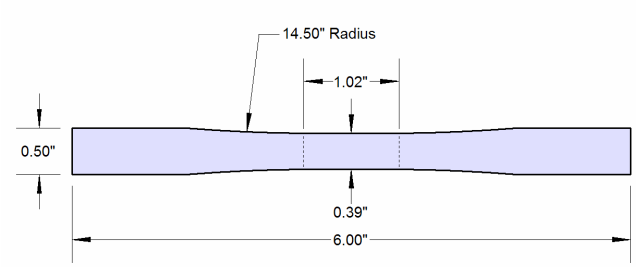

Figure 3. NASA Glenn MMC dogbone specimen.

(a)

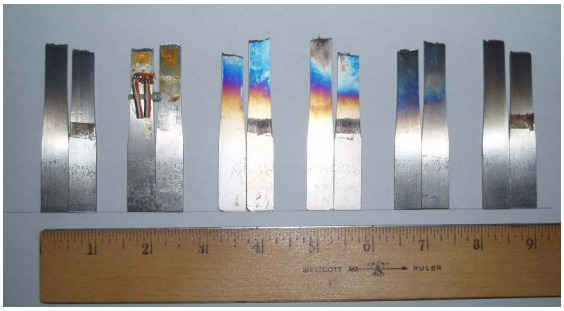

(b)

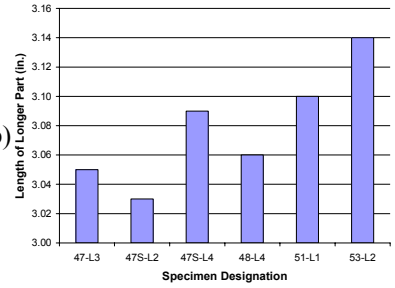

Figure 4. (a) Six failed longitudinal SiC/Ti-21S composite tensile specimens. (b) Plot of lengths of the longer part of the six failed specimens.

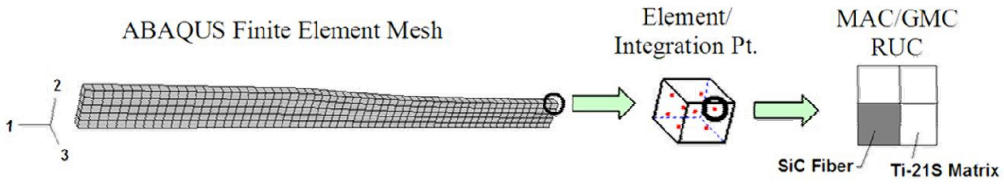

Figure 5. ABAQUS finite element mesh of the dogbone specimen and MAC/GMC RUC operating at each integration point.

that indicated the adequacy of the stress fields produced by this mesh. The simulated specimen has a total thickness of 0.125 in. and is subjected to symmetric boundary conditions on the three appropriate faces. Simulated displacement controlled loading is applied as an imposed $x_1$displacement on the positive x_1 face (see Fig. 5) at a rate of 3×10^{-4} in./s. We consider a 33% volume fraction unidirectional longitudinal composite specimen with continuous fibers oriented in the x_1-direction.

Utilizing the FEAMAC code, which couples the MAC/GMC micromechanics code with ABAQUS as described in Section 2.1, the composite material occupying each element is modeled via a GMC repeating unit cell (RUC). It has been shown (Bednarcyk and Arnold, 2001) that for longitudinal loading (i.e., loading along the fiber direction), the simplest composite RUC, consisting of 4 subcells is sufficient to capture the material response of SiC/Ti. As such, this 2×2 RUC (as shown in Fig. 5) has been employed to model the composite material response at each integration point of each element of the ABAQUS mesh. Note that, because each element contains eight integration points, the MAC/GMC micromechanics code is called 2400 times per iteration per increment in the FEAMAC simulation. The need for a highly efficient micromechanics approach such as GMC is thus obvious for performing multiscale simulations such as these.

On the local scale within the MAC/GMC input files, which define the composite material details, in addition to the geometry of the composite RUC, material properties for the fiber and matrix are required. The SiC fiber is treated as linearly elastic and isotropic with an elastic modulus of 57 Msi (393 GPa) and a Poisson ratio of 0.25. The Ti-21S matrix is treated as viscoplastic (as simulated with the GVIPS model, see Section 2.3) with an elastic modulus of 16.55 Msi (114.1 GPa) and a Poisson ratio of 0.365. The nine GVIPS viscoplastic material parameters for Ti-21S employed are given by Bednarcyk and Arnold (2001). It should be noted that temperature dependent material data is available for the SiC and Ti constituents, but that the current study considers only the isothermal response of the composite specimen at room temperature (23 °C). Furthermore, residual stresses from composite manufacture, which are known to affect the response of SiC/Ti, have been neglected in these analyses. As such, the presented results should be viewed as qualitative.

The final ingredient to the multiscale FEAMAC progressive failure analysis of the MMC specimen is the stochastic Curtin (1991) fiber failure model (described in Section 2.4). The Curtin model has been shown to work effectively within MAC/GMC to predict fiber failure in the SiC/Ti-21S composite material (Bednarcyk and Arnold, 2001). The model is applicable only to the fiber subcell in the RUC (see Fig. 5), and the model parameters are entered directly into the MAC/GMC input file associated with the element material. The employed Curtin model parameters (which are obtained from fiber strength statistics, see Fig. 9) are the fiber gauge length, L_0 = 1 in. (25.4 mm), diameter, d = 0.0056 in. (142 μm), characteristic strength, σ_0 = 609 ksi (4200 MPa), and Weibull modulus, m = 10. As noted in Section 2.4, the Curtin model predicts fiber stiffness degradation due to damage and complete effective fiber failure. MAC/GMC provides several options for treating complete fiber failure. Herein, upon complete failure, the fiber is given a very small stiffness (0.0001 times its original stiffness). Note that, based on the mesh shown in Fig. 5, along with the fiber diameter and composite fiber volume fraction, each element in the gauge section contains approximately 25 simulated fibers.

We first consider a simulation case in which the stochastic nature of the fiber failure process is captured only at the local level through fiber strength statistics incorporated within the Curtin model. In this case, the Curtin model parameters given above are assigned to all elements in the composite test specimen. The specimen is thus globally monolithic, exhibiting no structural scale material variation over the geometry. Locally, however, within each element, the fiber failure process is stochastic as damage and local failure are dictated by the Curtin model.

Figure 6 shows the global von Mises stress profile within the SiC/Ti specimen immediately prior to local fiber failure. This figure shows the stress concentrations that are inherent to dogbone type test specimens. At the specimen right edge, a strong minimum is observed at the start of the reduction section. A more mild maximum is present, as indicated in Fig. 6, at the transition from the reduction section to the gauge section (see also the dotted lines in Fig. 3). Because it is relatively mild, this maximum is difficult to see in the figure, but as indicated, it is an absolute maximum at node 67, which is just above the transition to the gauge section. This structural level concentration is exactly that discussed above which can lead to specimen failure outside the gauge section. Because a large reduction radius (14.5 in.) was employed in the NASA GRC specimen, this concentration is very mild. It has been shown that for smaller reduction radii, this concentration increases significantly (Worthem, 1990; Bednarcyk et al., 2005).

Figure 7 shows the progression of fiber failure within the composite specimen simulation. The fiber failure is quantified as a fraction of fiber damage within the elements; a fiber damage value of zero corresponds to an undamaged state, while a fiber damage value of 1.00 corresponds to complete failure of all fibers within an element. At this point it is worthwhile to summarize the process involved in the FEAMAC simulation whose results are shown in Fig. 7. Global

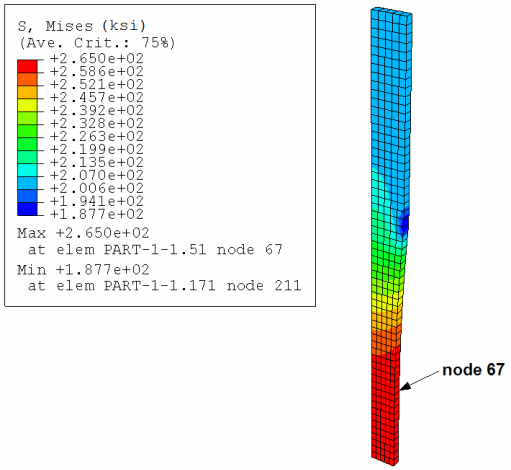

Figure 6. Global von Mises stress results for the longitudinal 33% SiC/Ti-21S specimen at an applied end displacement level of 0.02371485 in. (time = 79.0495 s – just prior to local fiber failure).

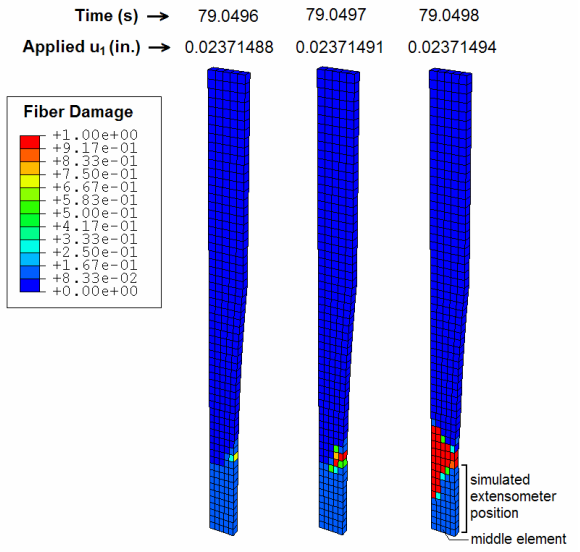

Figure 7. Local fiber damage fraction as a function of time as fiber failure progresses within the longitudinal 33% SiC/Ti-21S specimen.

incremental displacement loading is applied on the specimen, and ABAQUS solves the structural problem to determine the stress and strain fields throughout the specimen. The strains and strain increments at each integration point are then passed to MAC/GMC (through ABAQUS' UMAT subroutine), which performs a micromechanics analysis given the composite local geometry and constituent properties (see Fig. 5). Within MAC/GMC, the integration point strains are localized to the level of the fiber and matrix constituent subcells, which allows determination of the viscoplastic behavior of the matrix and the damage/failure behavior of the fiber. The local response of the fiber and matrix subcells are then homogenized within MAC/GMC to obtain new stresses and a new stiffness matrix (which may have changed due to the imposed strain increment and additional damage accumulation) for the composite at each particular integration point. This information is passed back to ABAQUS (through the UMAT subroutine), which can then impose the next increment of the applied global loading. This multiscale approach enables the effects of damage, failure, and inelasticity, and the associated redistribution within the RUC, to impact the global specimen response. When a particular integration point experiences fiber failure its stiffness is significantly reduced, which causes it to shed load. This load must then be carried by other integration points that remain intact and may cause failure to progress, as shown in Fig. 7.

Several important observations can be made from Fig. 7. First, the specimen failure initiates at the free edge exactly at the location of the stress concentration shown in Fig. 6. This occurs because, as stated above, there is no variation whatsoever of the composite material properties over the specimen. Therefore, even a slight concentration, like that occurring at the transition to the specimen gauge section, will necessarily cause the initiation of specimen failure. Second, after

initiation, the fiber failure progresses through the specimen very quickly (in three increments), as indicated by the time and applied displacement values shown at the top of the figure. This is because prior to failure initiation at the specimen edge, the fibers in nearby elements are themselves close to failing. Thus, once the first few integration points fail and shed load, the surrounding integration points fail in quick succession. It should be noted that complete fiber failure through the specimen, as depicted in Fig. 7, does not truly represent complete separation in the simulation because there remains matrix material subcells intact within the RUCs (see Fig. 5). A matrix failure criterion can be added to the simulation within MAC/GMC to model complete failure. However, tensile failure of longitudinal SiC/Ti specimens is known to be dominated by fiber failure.

Figure 8 shows simulated stress-strain curves for the SiC/Ti composite. Two curves are plotted for the FEAMAC simulation of the specimen, one representing a simulated extensometer measurement, and the other representing the local stress-strain response of an integration point within the middle element of the specimen (see Fig. 7). To obtain the strain history for the simulated extensometer curve, the x_1 displacement at the top of the gauge section (at the specimen free edge) was compared to that at the specimen middle, and the difference divided by the length between these points (0.51 in.). This simulates the reading from an (approximately) 1 in. extensometer, which would be clipped on the edge of the specimen as shown in Fig. 7. The stress history for the simulated extensometer curve in Fig. 8 was determined by first obtaining the centroidal longitudinal stress averaged over the top five elements, and then concentrating the values due to the gauge section reduction (i.e., multiplying by 0.5/0.39). This stress history thus simulates load cell data that would be obtained in an actual tensile test performed on the specimen. The middle element stress-strain curve in Fig. 8 was obtained from integration point level FEAMAC output. The final curve plotted in Fig. 8 is from a stand alone MAC/GMC simulation of the SiC/Ti composite material (as represented by the 2×2 RUC, see Fig. 6) subjected to strain controlled loading analogous to the initial strain rate experienced in the specimen gauge section.

Figure 8 shows that, in the linear elastic range, all three curves are nearly identical, as is expected. Near the curves' peaks, all three curves become nonlinear due mainly to the onset of Curtin fiber damage and partly to a small amount of matrix inelasticity. The curves applicable to the simulation of the specimen exhibit slightly more nonlinearity due to the presence of the concentrations which are absent in the stand alone MAC/GMC simulation. Upon the onset of complete fiber failure, all three curves diverge widely. Lacking any stress concentrations, the stand alone MAC/GMC curve achieves a higher stress level prior to failure, but then, upon complete failure of the single fiber in the RUC, the stiffness drops significantly, as does the stress level (by 40%, as expected from the RUC stiffness reduction). After this large drop, the composite can still carry additional load as the applied strain is increased due to the continuity of the (flowing) matrix. The curve associated with the middle element also unloads stress upon initiation of complete fiber failure, however, unlike the stand alone MAC/GMC curve, this curve follows an unloading path back towards the origin. This can be explained by the fact that the middle element experiences only a small amount of fiber damage (see Fig. 7) because it is not near the failure zone. As such, when the failure zone progresses quickly through the specimen above the middle element, the load carried by the middle element decreases as does the strain. This phenomenon is much like the response of an undamaged link adjacent to a link in a chain that fails in tension. Finally, the simulated extensometer curve exhibits a decrease in stress along with

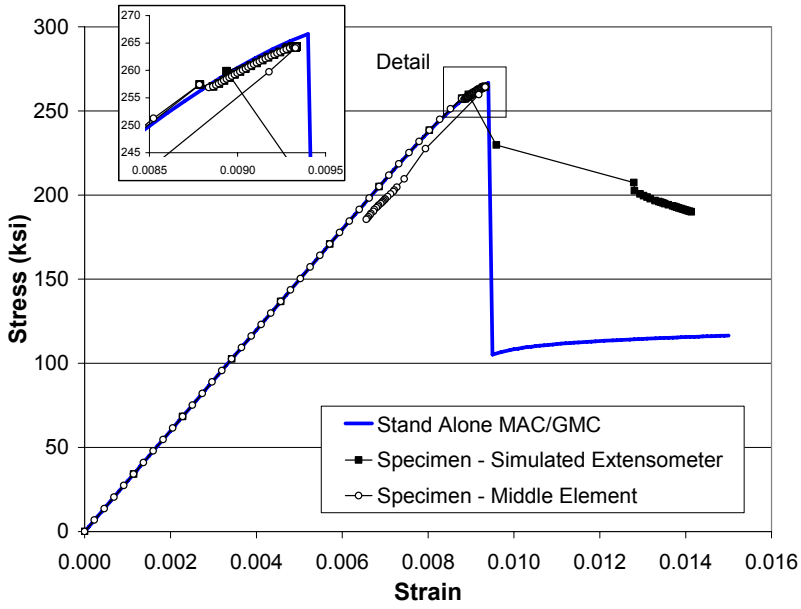

Figure 8. Simulated stress-strain response of the longitudinal 33% SiC/Ti-21S specimen.

an increase in strain. This is caused by the specimen's decreased ability to carry additional load as the failure progresses coupled with the rapid increase in deformation of the failure zone, part of which is encompassed within the simulated extensometer measurement (see Fig. 7). Note that the simulated extensometer and stand alone MAC/GMC simulations predict very similar ultimate strengths for the composite; 264.3 ksi (1822 MPa) and 266.6 ksi (1838 MPa), respectively.

It is clear from Fig. 7 that the multiscale stochastic FEAMAC simulation of the MMC specimen has predicted failure outside of the gauge section, which, as illustrated in Fig. 4, does not typically occur with the NASA GRC MMC tensile specimen. This shortcoming is due to the inappropriate implementation of the fiber strength variability exclusively at the local level. In order to more realistically simulate the SiC/Ti tensile specimen progressive failure, it is necessary to account for the realistic fiber strength distribution on the structural level. This has been accomplished by varying the Curtin model parameters over the specimen geometry. An obvious choice for this variation is the Curtin model characteristic strength, σ_0. Providing different elements with different values of this parameters, in essence allows the elements to damage and fail at different fiber stress levels as desired.

To distribute the characteristic strength spatially, 30 user materials were associated with the mesh. Each material was defined by a MAC/GMC input file with different σ_0 value chosen according the vendor-supplied fiber strength histogram shown in Fig. 9 (Specialty Materials, Inc., 1991). First,

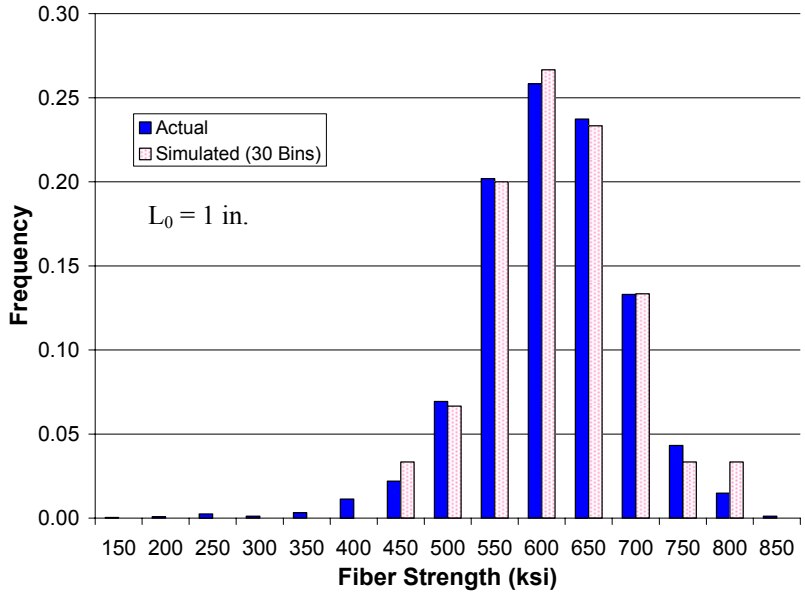

Figure 9. Fiber strength histogram for SCS-6 SiC fibers. The actual data is vendor-supplied, while the simulated data refers to the distributed characteristic strength.

the number of user materials having σ_0 values in each 50 ksi range (see the horizontal axis of Fig. 9) was determined in order to provide a good match with the actual fiber strength distribution (as shown in Fig. 9). If only one material's σ_0 value was located within a particular 50 ksi range, the characteristic strength was chosen as the middle of that range. Otherwise, the characteristic strength values for the materials were evenly distributed within the applicable 50 ksi range. As shown in Fig. 9, the 30 σ_0 values provide an excellent match with the actual fiber strength histogram.

The other important Curtin model parameter that must be considered to obtain the correct fiber strength statistics is the Weibull modulus, *m*, as this affects the shape of the fiber strength distribution. One might consider using a constant value of *m* for all values of σ_0. However, when summing over all fibers, this does not reproduce the correct overall fiber strength distribution. This can be remedied by allowing each user material to have a distinct Weibull modulus value. A simple computer program was written to optimize the Weibull modulus values in order to provide the best correlation of the combined fiber strength distribution of all 30 user materials with the actual fiber strength distribution.

Now, with 30 user materials (represented by 30 MAC/GMC input files) whose Curtin model data cumulatively represent the fiber strength statistics accurately, the 300 elements within the specimen were randomly distributed to the user materials (with ten elements per material, all ten having identical properties). The random distribution was accomplished via a simple computer

program. The resulting distribution of Curtin model characteristic strengths, σ_0, over the specimen geometry is shown in Fig. 10. This model, with its fiber strength distribution now varying over the specimen, was subjected to the identical simulated tensile test considered previously in the non-distributed case.

Results for the progressive failure simulation of the spatially distributed fiber strength statistics specimen are given in Fig. 11. In this simulation, failure initiated not at the stress concentration (see Fig. 6), but rather in the middle of the specimen within the gauge section in an element with a low characteristic strength (see Fig. 10). Subsequently, failure across the specimen did not progress rapidly. Rather, global loading on the specimen continued for 0.6 seconds before the fibers in another weak element, again within the specimen gauge section, failed. The adjacent element, located on the specimen edge, then failed rapidly as this element also contained relatively weak fibers. This established failure path across the specimen was then arrested due to the presence of a stronger element (see Fig. 10), and it took 2.64 seconds of additional global loading before further fiber failures occurred in elements along the initial failure path. Failures then progressed in rapid succession along this path through the specimen, signaling final failure.

Figure 12 provides a comparison of stress-strain curves from the spatially distributed fiber strength statistics case with the non-distributed case described previously and the stand alone MAC/GMC simulation. The difference between the middle element curve and the simulated extensometer curve is similar to that observed in Fig. 8 for the non-distributed case. However, a striking difference is evident when comparing the simulated extensometer curves between the distributed and non-distributed cases. The distributed simulation predicts an ultimate strength of 210.4 ksi (1451 MPa) compared to a value of 264.3 ksi (1822 MPa) for the non-distributed simulation. This

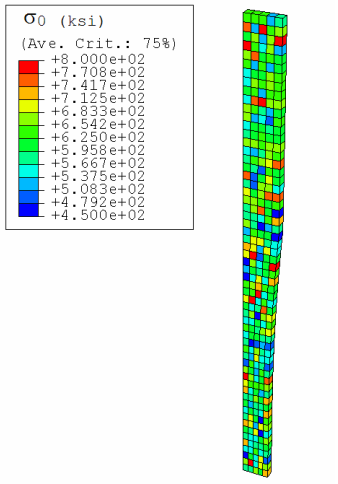

Figure 10. Distribution of fiber characteristic strengths over the specimen geometry. Note that the Weibull modulus also varies over the geometry.

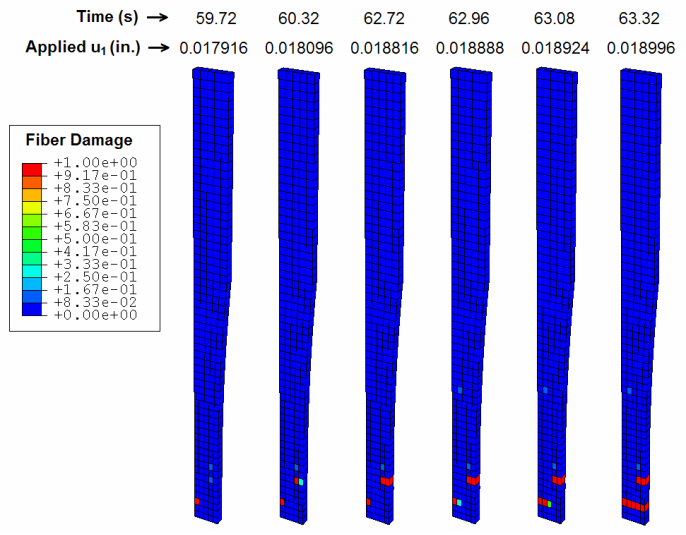

Figure 11. Local fiber damage fraction as a function of time as fiber failure progresses within the longitudinal 33% SiC/Ti-21S specimen with spatially distributed fiber strength statistics.

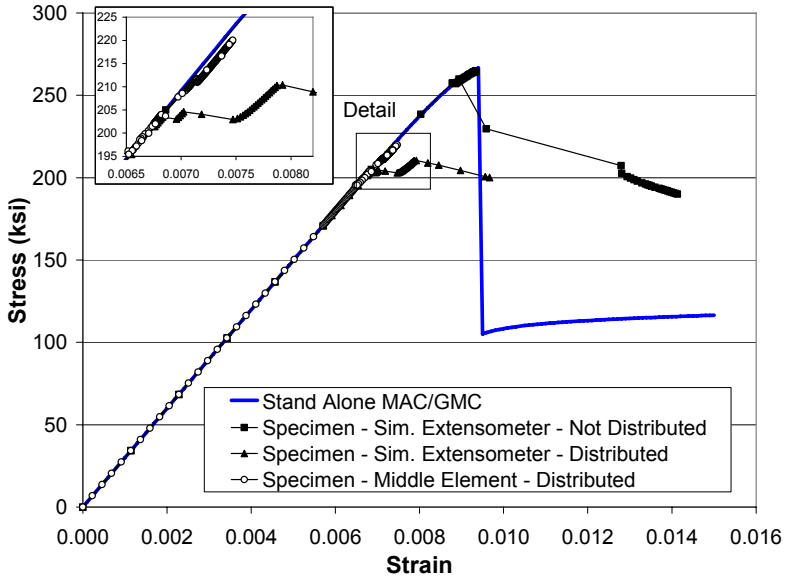

Figure 12. Simulated stress-strain response of the longitudinal 33% SiC/Ti-21S specimen with spatially distributed and non-distributed fiber strength statistics.

represents a difference of more than 25%. Furthermore, because the progression of fiber failure was arrested prior to reaching the ultimate stress in the non-distributed simulation, the specimen was able to carry additional load after failure initiation, resulting in the stepped curve in Fig. 12.

Because the simulation that employed distributed fiber strength statistics failed within the gauge section, which, as is shown in Fig. 4, is typical of the GRC MMC tensile specimen, it can be said that this simulation is more qualitatively accurate compared to the non-distributed model. To assess the quantitative accuracy via comparison with experimental results, additional work is necessary to recalibrate certain model parameters and incorporated residual stresses in the FEAMAC simulation.

4. Conclusions

A framework for the multiscale analysis of composite structures has been presented. By combining the powerful and efficient micromechanics capabilities of MAC/GMC with the robust structural analysis capabilities of ABAQUS, FEAMAC enables analysis down to the level of the fiber and matrix constituents on the fly at each integration point during each FEA loading increment and iteration. The availability of the constituent fields throughout the composite structure enables incorporation of nonlinear inelastic, damage, and failure models that operated on the monolithic constituent scale. This consistent multiscale framework circumvents the need for complex, multiaxial, anisotropic damage and constitutive models that are required to operate on the macro scale for nonlinear composite structural analyses.

The FEAMAC capabilities were employed to perform a multiscale stochastic analysis of the progressive failure of a longitudinal titanium matrix composite tensile specimen. The titanium matrix inelastic behavior was modeled using a GVIPS viscoplasticity model, while the fiber damage and failure behavior was modeled using the Curtin statistical fiber breakage model, both of which operated on the micro scale within MAC/GMC. It was shown that accounting for statistics at only the micro scale, with the damage and failure parameters applied uniformly at all integration points, lead to predicted failure at the highest structural stress riser. However, spatially randomizing the fiber strength statistics throughout the specimen (which appears to be physically justified) enabled realistic gauge section failure, and resulted in a significantly lower specimen tensile strength prediction along with more progressive failure.

5. References

1. Aboudi, J. "The Generalized Method of Cells and High-Fidelity Generalized Method of Cells Micromechanical Models – A Review," Mechanics of Advanced Materials and Structures, vol. 11, pp. 329-366, 2004.

2. Arnold, S. M., A. F. Saleeb, and M. G. Castelli, "A Fully Associative, Nonisothermal, Nonlinear Kinematic, Unified Viscoplastic Model for Titanium Alloys," NASA TM 106926, NASA Glenn Research Center, Cleveland, OH, 1994.
3. Bednarcyk, B. A. and S. M. Arnold, "Micromechanics-Based Deformation and Failure Prediction for Longitudinally Reinforced Titanium Composites," Composites Science and Technology, vol. 61, pp. 705-729, 2001.
4. Bednarcyk, B. A. and S. M. Arnold, "MAC/GMC 4.0 User's Manual – Keywords Manual," NASA/TM–2002-212077/VOL2, NASA Glenn Research Center, Cleveland, OH, 2002.
5. Bednarcyk, B. A. and S. M. Arnold, "MAC/GMC 4.0 User's Manual – Example Problem Manual," NASA/TM–2002-212077/VOL3, NASA Glenn Research Center, Cleveland, OH, 2002.
6. Bednarcyk, B. A., S. M. Arnold, and L. M. Powers, "Micromechanics-Based FEA of Composite Structures," in Proc. The Eleventh International Symposium on Plasticity, January, Kauai, Hawaii, 2005.
7. Bowman, C. L., "Experimentation and Analysis of Mechanical Behavior Modification of Titanium Matrix Composites through Controlled Fiber Placement," Ph. D. Thesis, Department of Materials Science and Engineering, Case Western Reserve University, Cleveland, OH, 1999.
8. Collier Research Corp., HyperSizer Structural Sizing Software User' Manual, Hampton, VA, 2005.
9. Curtin, W. A., "Theory of Mechanical Properties of Ceramic-Matrix Composites," Journal of the American Ceramics Society, vol. 74, pp. 2837-2835, 1991.
10. Lerch, B. A., Personal Communication, NASA Glenn Research Center, Cleveland, OH, 2005.
11. Paley, M. and J. Aboudi, "Micromechanical Analysis of Composites by the Generalized Cells Model," Mechanics of Materials, vol. 14, pp. 127-139, 1992.
12. Pindera, M.-J. and Bednarcyk, B.A., "An Efficient Implementation of the Generalized Method of Cells for Unidirectional, Multi-Phased Composites with Complex Microstructures," Composites: Part B, vol. 30, pp. 87-105, 1999.
13. Spencer, A. J. M., Deformation of Fibre-Reinforced Materials, Oxford University Press, New York, 1972.
14. Specialty Materials, Inc., Lowell, MA, 1991.
15. Wilt, T.E., "On the Finite Element Implementation of the Generalized Method of Cells Micromechanics Constitutive Model," NASA Contractor Report 195451, 1995.
16. Worthem, D. W., "Flat Tensile Specimen Design for Advanced Composites," NASA Contractor Report 185261, NASA Glenn Research Center, Cleveland, OH, 1990.